NANO LETTERS
Letter
pubs.acs.org/NanoLett

Rational Design of Amorphous Indium Zinc Oxide/Carbon Nanotube Hybrid Film for Unique Performance Transistors

Xingqiang Liu,[†] Chunlan Wang,[†] Bo Cai,[†] Xiangheng Xiao,[†] Shishang Guo,[†] Zhiyong Fan,*[,‡] Jinchai Li,[†] Xiangfeng Duan,[§] and Lei Liao*[,†]

[†]Department of Physics and Key Laboratory of Artificial Micro- and Nano-structures of Ministry of Education, Wuhan University, Wuhan 430072, China

[‡]Department of Electronic & Computer Engineering, Hong Kong University of Science & Technology, Hong Kong SAR, China

[§]Department of Chemistry and Biochemistry, University of California, Los Angeles, California 90095, United States

Supporting Information

ABSTRACT: Here we report unique performance transistors based on sol−gel processed indium zinc oxide/single-walled carbon nanotube (SWNT) composite thin films. In the composite, SWNTs provide fast tracks for carrier transport to significantly improve the apparent field effect mobility. Specifically, the composite thin film transistors with SWNT weight concentrations in the range of 0−2 wt % have been investigated with the field effect mobility reaching as high as 140 $cm^2/V{\cdot}s$ at 1 wt % SWNTs while maintaining a high on/off ratio $\sim 10^7$. Furthermore, the introduction SWNTs into the composite thin film render excellent mechanical flexibility for flexible electronics. The dynamic loading test presents evidently superior mechanical stability with only 17% variation at a bending radius as small as 700 μm, and the repeated bending test shows only 8% normalized resistance variation after 300 cycles of folding and unfolding, demonstrating enormous improvement over the basic amorphous indium zinc oxide thin film. The results provide an important advance toward high-performance flexible electronics applications.

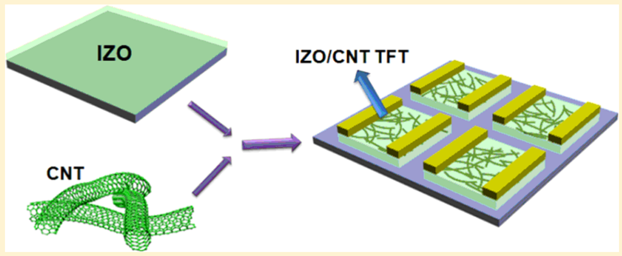

KEYWORDS: *Indium zinc oxide, carbon nanotubes, transistor, high mobility, flexible*

Thin film transistors (TFTs) have broad applications for flexible electronics and information display. In the past, although the silicon-based TFTs have been primarily used for these applications,[1,2] they all have been suffering from a number of limitations, including poor mechanical flexibility and/or indispensable high-temperature deposition processes, and particularly, much poorer performance as compared to the devices fabricated on a single crystalline wafer. Typically, α-Si TFT devices demonstrate a mobility of ~ 1 $cm^2/V{\cdot}s$ for display application,[3,4] which limits their performance. The emerging organic TFTs can be processed essentially at room temperature but are also limited by poor mobility (~ 1 $cm^2/V{\cdot}s$) and poor stability in the long run.[5] So there is more and more research exploring new materials for higher performance devices.[6,7] With excellent transparency, high stability, and low-temperature processes, amorphous metal oxide materials have drawn considerable attention for potential applications in transparent and flexible electronics, such as touch display panels. To date, most metal oxide TFTs have been fabricated with amorphous indium zinc oxide (α-IZO), zinc indium tin oxide,[8] ZnO,[9] In_2O_3,[7] indium gallium zinc oxide,[10−12] or some other oxide semiconductors as channel materials by the sol−gel route, with the performance approaching that of crystalline silicon based materials.[13] Particularly for α-IZO TFTs prepared via the solution route, they have advantages over the vacuum deposition processes in terms of simplicity, cost, and scalability. High κ self-assembled nanodielectrics has been explored as the gate insulator to fabricate amorphous metal oxide TFTs with the demonstrated mobility as high as 120 $cm^2/V{\cdot}s$.[6] However, thermal stability is a key challenge to self-assembled nanodielectric development.

To implement high-performance electronics, materials with a high carrier mobility are required. With regard to the original α-IZO TFTs, the carrier mobility is too poor to promise potential applications (usually 1−10 $cm^2/V{\cdot}s$ on SiO_2 back gate).[11,14−16] So it is important to further improve it in terms of mobility. On the other hand, although the mechanical flexibility of α-IZO thin film is better than that of crystalline phase, there were still reports on the drastic performance degradation after repetitive bending; thus, it is not satisfactory for practical flexible electrics, when compared with organic TFTs.[17] In the past, single-walled carbon nanotubes (SWNT)s have attracted substantial research interest for flexible electronics applications owing to their unique mechanical and electrical properties. They are among

Received: April 3, 2012
Revised: June 7, 2012
Published: June 13, 2012

the strongest fibers in the world, with a Young's modulus in the range of 1−2 TPa, fracture stress of 50 GPa, and a high mobility ~10 000 $cm^2/V \cdot s$.[18] Depending on their chirality and diameter, a SWNT can behave as either a metallic material (*m*-SWNTs) or a semiconductor material (*s*-SWNTs).[19] Nevertheless, there still lacks an effective method to control the chirality and assembling a large number of SWNTs deterministically to realize scalable device/circuit fabrication.

Herein, we propose a novel approach that addresses both the unsatisfactory mobility and mechanical behaviors of the α-IZO thin film, through using a hybrid material structure consisting of SWNTs embedded directly into the α-IZO thin film via a simple spin-coating process, which significantly improves electrical properties and mechanical behaviors of the thin films. In addition, this process is demonstrated to be compatible with different types of substrates.

Figure 1a presents an analogy of the design concept: with a high mechanical strength and toughness, reinforced concrete,

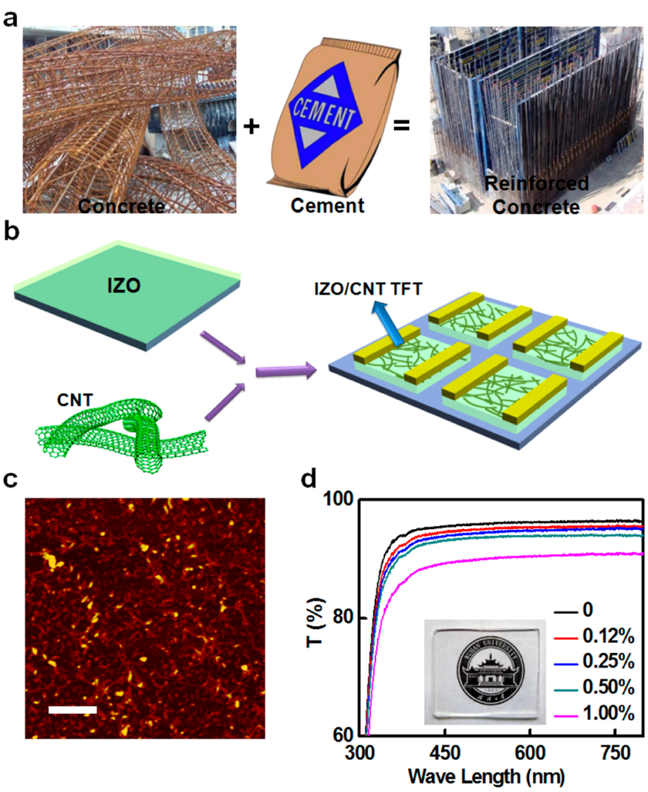

Figure 1. Schematic representation of the TFT structure employed in this study. (a) The design conception of the nanosystem and (b) combination of α-IZO and SWNTs to fabricate the hybrid TFT array. (c) The atomic force microscopy image of the surface view of the hybrid thin film; the scale bar is 1 μm. (d) The ultraviolet−visible transmission spectrum of the hybrid thin film with the weight percent of SWNTs systematically from 0 to 1 wt %; the inset image is the optical image for the α-IZO/SWNTs hybrid thin film.

which is made of concrete and cement, is widely used in the construction industry. Concrete is a brittle material and is strong in compression; however, it is weak in terms of tension. On the other hand, steel has a high tensile strength. When completely surrounded by the hardened concrete mass it forms an integral part to interlock both materials, forming "Reinforced Concrete" (Figure S1, Supporting Information). Similarly, we propose the model of hybrid thin film composed of SWNTs and α-IZO. On one hand, SWNTs could give rise to dramatic enhancement of mechanical behaviors; on the other hand, by utilizing the sol−gel route SWNTs are embedded into α-IZO to form a three-dimensional (3-D) evenly distributed hybrid thin film which serves as electron-conducting channels. The hybrid thin film is composed of a large number of nanotubes in the form of a random network embedded in the α-IZO block; hence the 2/3 inherent *s*-SWNTs were passivated, leading to an even metallic SWNTs network in the hybrid nanosystem.[20] So the superior transporting channels result in a significant improvement on mobility. Figure 1b shows the fabrication process of a hybrid TFT array. Briefly, SWNTs (>90 wt %, 0.5−2 μm in length, AlphaNano Technology Co., Ltd.) were added into 2-methoxyethanol (2-ME) and then ultrasonized to achieve uniform dispersion in the solution, labeled as solution A. Then a 0.03 M mixture of zinc acetate dihydrate $[Zn(OAc)_2 \cdot 2H_2O]$ and indium nitrate hydrate $[In(NO_3)_3 \cdot 4H_2O]$ was used as the sol−gel precursor; the mole ratio of In/Zn was fixed at 1:1, which were dissolved in 2-ME. Monoethanolamine (EA) was added with the mole ratio of In/EA = 1:10 and then stirred for 1 h at room temperature to form stable IZO precursor solutions. Thereafter, solution A with the SWNT/IZO weight concentration ranging systemically from 0 to 1% was added into IZO precursor solutions. Finally, ultrasonication was performed for 2 h to form homogeneous hybrid thin film precursor solutions, and the total volumes of the solutions were all fixed at 50 mL. The precursor solution was then spin-coated onto SiO_2 (300 nm) coated *p*-Si substrate (TFT back-gate contact) at 2400 rpm for 60 s and prebaked on a hot plate at 150 °C for 10 min to remove the organic solvent. After prebake, the films were cooled to room temperature, and the aforementioned processes were repeated subsequently. The as-prepared thin films were annealed on the hot plate at 350 °C for 40 min in the atmosphere. Finally, the 60 nm thick α-IZO/SWNTs thin films were obtained. A first photolithography and wet etch process was carried out to define the as-prepared thin film into isolated pads. Note that our back-gate device structure not only suppressed the gate leakage current but also reduced parasitic capacitance, both of which were essential for back-gate TFTs.[4,21,22] Subsequently, the second photolithography was conducted to pattern the source and drain, and the TFT structure was completed by the Cr/Au (15 nm/30 nm) evaporation and lift-off process.

The morphologies of the thin films are examined by atomic force microscopy. Figure 1c shows a 0.5 wt % α-IZO/SWNTs hybrid thin film, indicating that the film is compact, uniform, and reasonably smooth with a few overweight SWNTs dispersed randomly on surface. The Raman spectrum of the hybrid thin film also indicates the matched peaks of SWNT (Figure S2, Supporting). The ultraviolet−visible transmission spectrum demonstrates that the hybrid thin films have good transparency in the visible region (Figure 1d). The inset image in Figure 1d shows an optical image and the transparent nature of the α-IZO/SWNT film on glass. Therefore, the amorphous hybrid thin film prepared in this study is a good candidate for fabricating transparent devices.

After TFTs fabrication, the back-gated devices were evaluated in ambient conditions. The $I_{ds}-V_g$ curves of α-IZO based TFTs with SWNT weight concentrations from 0 to 1% were measured (Figure 2a−c). The channel length and width we used here are 20 μm and 75 μm, respectively, with a 300 nm thick SiO_2 gate insulator; the resulting field effect carrier mobility in the α-IZO based TFTs increases from 1.9 $cm^2/V \cdot s$

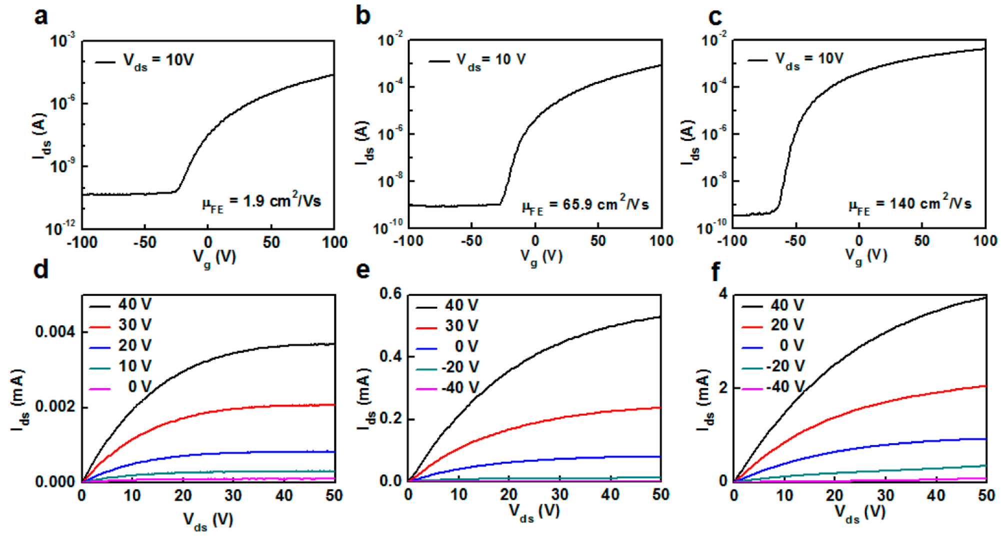

Figure 2. Electrical characteristics of the α-IZO/SWNT hybrid TFTs with different SWNT concentrations from 0 to 1 wt %. (a−c) Transfer characteristics (with I_{ds} plotted logarithmically) at V_{ds} = 10 V: (a) 0 wt %, (b) 0.5 wt %, (c) 1 wt %. (d−f) Output characteristics: (a) 0 wt %, (b) 0.5 wt %, (c) 1 wt %.

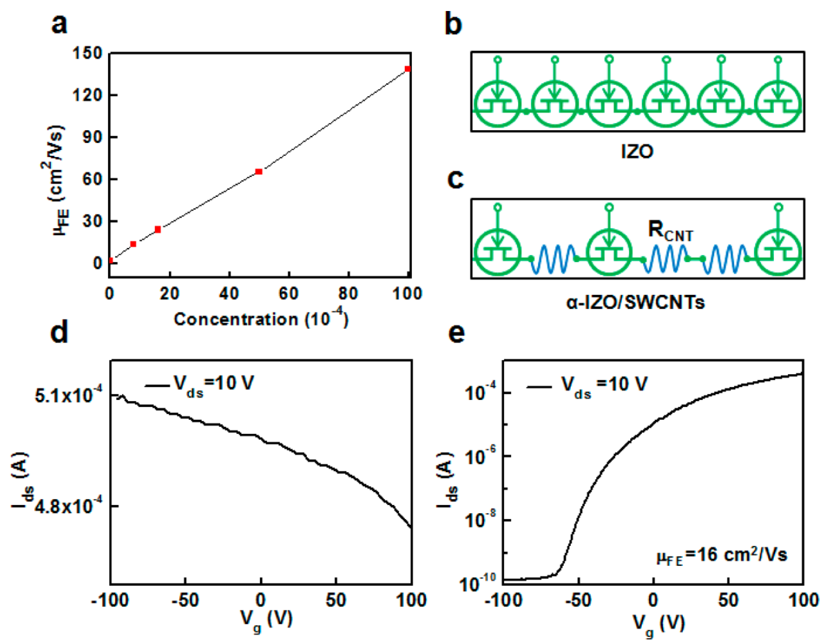

Figure 3. (a) Mobility of the α-IZO/SWNT TFTs as a function of the concentration of SWNTs. (b) The simplified circuit diagrams of the microstructure of the pristine α-IZO TFTs and (c) the hybrid α-IZO/SWNT TFTs. Some SWNTs replace α-IZO in the hybrid thin film, and the superior tracks are used to achieve carrier transport with less scatter. (d) The high concentration SWNTs in the α-IZO/SWNT hybrid thin film lead to a highly conductive and weak p-type field effect. (e) The transfer characteristic of the α-IZO/MWNT TFT with 0.5 wt % MWNTs; compared with the equal concentration α-IZO/SWNTs film, the mobility is quite smaller.

for pristine film to a high mobility of 140 cm^2/V·s for the hybrid film with 1 wt % SWNTs. In addition, the I_{ds}−V_{ds} curves display a clear linear regime at low voltages (Figure 2d−f), indicating ohmic contacts formed between the Cr/Au electrodes and hybrid thin film. The clear pinch-off and I_{ds} saturation indicate that the carrier transport in active channels is completely controlled by the gate potential. As mentioned in the former, SWNTs replaced α-IZO in the block and provided fast tracks for carrier transport with less scatter in the hybrid thin film.[23] Due to the number of SWNTs imbedded into the hybrid thin film increased with the SWNTs weight concentration, the increasing SWNT weight concentration leads to the enhancement of both transfer and output characteristics, with the on/off ratio enhanced from ∼5 × 10^5 to ∼1.3 × 10^7.

The critical effect of the SWNTs used in the precursor solutions is demonstrated in the field effect mobility versus SWNTs weight concentration, which is shown in Figure 3a. Also it demonstrates an approximately clear linear relationship between them. To explain the improvement on TFT performance with incorporating SWNTs, we present equivalent circuit diagrams in Figure 3b,c. The transconductance can be obtained in the form of $g_m = (\partial I_d/\partial V_g)$, and considering the totally collective effect,

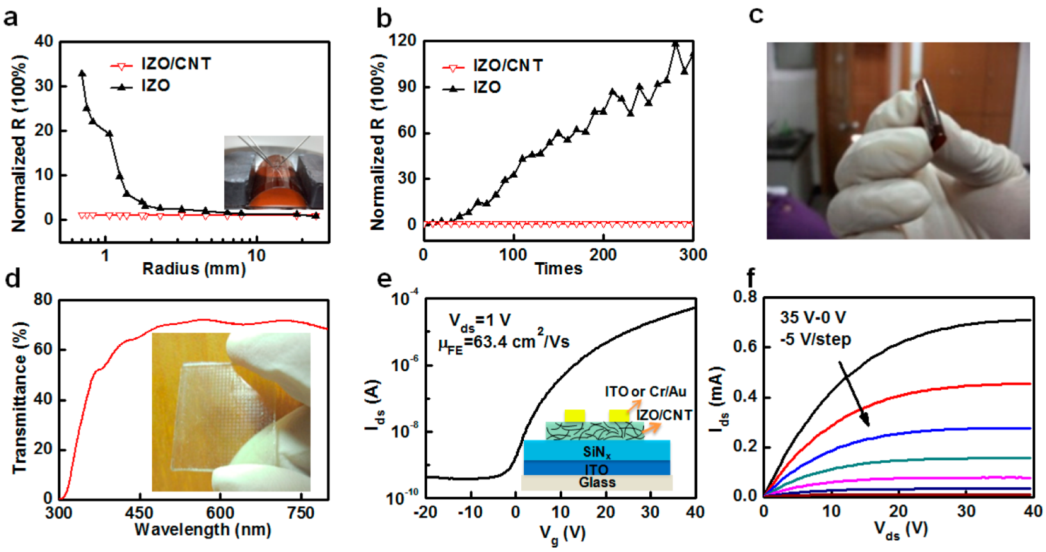

Figure 4. Plot showing the bending effect on the normalized resistances of α-IZO and α-IZO/SWNTs thin film. (a) The loading test of the dynamic resistance as bending. (b) The normalized resistance as a function of the folded times. (c) The photograph that measures the repeated bending performance. (d) The ultraviolet–visible transmission spectrum of the real device, and the inset is the optical image. (e and f) Electrical characteristics of the transparent 0.5 wt % α-IZO/SWNTs TFT fabricated on ITO coated glass; the inset in e is the schematic diagram of the transparent TFT, where the fabricated device shows a reasonable field effect mobility of 63.4 cm^2/V·s.

$$g_m = \frac{\Delta \frac{V_{ds}}{R_{ch}}}{V_g - V_T} \approx \frac{\frac{V_{ds}}{R_{on}} - \frac{V_{ds}}{R_{off}}}{V_g - V_T} \tag{1}$$

The pristine α-IZO TFT can be regarded as n parts individual small FETs connected in series, shown in Figure 3b. In this case, each FET has a resistance R_i at the ON state. As the on/off ratio of the fabricated devices are all larger than 10^4, overall $R_{off} > 10^4 R_{on} = 10^4 nR_i$, hence

$$g_{m1} = \frac{\frac{V_{ds}}{R_{on}} - \frac{V_{ds}}{R_{off}}}{V_g - V_T} \approx \frac{V_{ds}}{V_g - V_T} \frac{1}{nR_i} \tag{2}$$

On the other hand, the equivalent circuit for the hybrid thin film is depicted in Figure 3c, in which some SWNTs "short" α-IZO FETs in the hybrid thin film.[24] Compared with R_i, the resistance of an individual SWNT we used here can be ignored. Then, assuming that m ($m < n$) parts of the α-IZO are shorted by SWNTs; therefore,

$$g_{m2} = \frac{\frac{V_{ds}}{R_{on}} - \frac{V_{ds}}{R_{off}}}{V_g - V_T} \approx \frac{V_{ds}}{V_g - V_T} \frac{1}{(n - m)R_i} \tag{3}$$

Hence

$$\mu_2/\mu_1 = g_{m2}/g_{m1} = \frac{n}{n - m} \tag{4}$$

$$\mu_2 = \frac{n}{n - m}\mu_1 \tag{5}$$

As the SWNT molar concentration is close to the precursor of α-IZO, this leads to the number of SWNTs incorporated in the hybrid system approaching to that of the α-IZO parts; hence the measured mobilities demonstrate a close to linear dependence on the SWNTs concentration shown in Figure 3a. This clearly explains that the field effect mobility increases with the concentration of SWNTs. In accordance with this rationale, we intended to exploit the limitations of the achievable mobility. Figure 3d shows the transfer characteristics as we doubled the SWNTs concentration to 2 wt % corresponding to the largest mobility we have obtained (140 cm^2/V·s). Interestingly, the film presents high conductance but a weak p-type field effect, indicating the SWNTs are starting to make a fully percolation network to dominate the charge transport. The pristine-SWNT devices have been fabricated by electron beam lithography (JEOL SEM with an NPGS system), the electrical properties are similar with that of 2 wt % SWNT into α-IZO film (shown in Figure S3 of the Supporting Information). As coessential materials, we also demonstrated that the MWNTs were valid for improving the mobility of α-IZO thin film as well, shown in Figure 3e. However, as both the volume and mass of an individual MWNT are much larger than SWNT, so the numbers of MWNTs embedded into the hybrid system were much less than SWNTs with the same weight concentration. Thus the mobility of 0.5 wt % α-IZO/MWNTs TFT is lower than that of equal weight concentration α-IZO/SWNT TFTs that we have demonstrated.

To confirm the critical role of SWNTs for achieving excellent device mechanical behaviors, we fabricated two pairs of α-IZO and α-IZO/SWNT (with 0.5 wt % SWNTs) devices both on polyimide substrate via the same processes. Generally, the lack of SWNTs in the pristine α-IZO thin film led to more fragility. Dynamic loading tests were carried out (see the inset of Figure 4a). The actual bending radius of the loaded substrates was measured by fitting circles to images taken by an optical camera mounted facing the edge of the film. All devices under test were characterized at a specific bending radius by measuring the channel resistance and then normalized to the strainless state. It is evident that, as the radius decreased to less than 2 mm, the conductance of pristine α-IZO thin film deteriorated dramatically, until it reached the scrapped state of more than 3200% variation, when the substrate was pushed at the smallest radius of 700 μm (the bending radius is limited by the rigid areas within the substrate, and the thickness of the substrate is about 200 μm). In contrast, the hybrid thin film exhibits much better mechanical stability with the largest variation of only 17%, as shown in Figure 4a. To our knowledge, the smallest bending radius of α-IZO/NT film in this work is also the smallest among most of oxide film transistors (~10 mm).[14] Notably, it is even of comparability with the organic TFTs that were demonstrated to possess extreme bending stability.[17] The repeated bending test of the devices was evaluated by bending the substrate into an ultrasmall radius along the axis running exactly through the channel, with the direction of the bending-induced strain aligned perpendicularly to the direction of the current flow from drain to source (as shown in Figure 4c). Figure 4b shows the normalized channel resistance as a function of bending cycles. As it can be seen, the variation is less than 8% for the α-IZO/SWNT hybrid thin film, which indicates the hybrid thin film devices are stable for a series of rigorous bending tests even after 300 cycles of repeated bending. However, the pristine α-IZO thin film showed quick performance degradation. To our knowledge, the overall mechanical performances reported here are among the best in the past research on amorphous metal oxide based devices.[14,25,26] All in all, the excellent performances, including high transparency, high mobility, and excellent mechanical stability greatly favor the potential applications of real high mobility flexible and transparent TFTs.

To fabricate transparent TFTs, 200 nm SiN_x was deposited on ITO glass by plasma enhanced chemical vapor deposition (the C−V curve of SiN_x is shown in Figure S4 of the Supporting Information, indicating a capacitance per unit area of 29.5 nF/cm^2), and then α-IZO/SWNT hybrid thin films with 0.5 wt % SWNTs were fabricated with the aforementioned processes, followed by photolithography process to define the source/drain patterns on the thin film. Eventually, the transparent TFTs array was fabricating after sputtering 50 nm ITO film. Figure 4d is the ultraviolet−visible transmittance spectrum of the real device, with the inset optical image indicating the transparency. The $I-V$ characteristics of a hybrid α-IZO/SWNT n-channel TFT are shown in Figure 4e,f. Accordingly, we have obtained the field effect mobility from $I_{ds}-V_g$ curve in Figure 4e, leading to a reasonable result of 63.4 cm^2/V·s, comparable to the TFTs fabricated on silicon oxide. This result indicates that the α-IZO/SWNT hybrid thin films used in this experiment are stable and could be generalized to other nanosystems to obtain transparent and flexible devices defined on some types of substrates.

In conclusion, we have demonstrated that the sol−gel processed α-IZO/SWNTs composite thin film shows promises as a transparent, flexible, and high mobility material. In the composite, SWNTs provide fast tracks for carrier transport to significantly improve the apparent field effect mobility. Furthermore, SWNTs render excellent mechanical flexibility for flexible electronics. Finally, we have successfully demonstrated the transparent TFTs by processing the composite thin film on commercial ITO glass substrate, which indicated our methods and materials were environmentally stable, compatible, and suitable for being generalized on other substrate for flexible and transparent electronics.

■ ASSOCIATED CONTENT

Supporting Information

Schematic diagram of the analogic design conception of reinforced concrete (Figure S1); Raman spectrum of SWCNTs and the hybrid thin film (Figure S2); electrical transfer characteristics of the pristine SWCNTs network (Figure S3); $C-V$ curve of the SiN_x insulator deposited by plasma enhanced chemical vapor deposition (Figure S4); electrical characteristics of the 1.5 wt% α-IZO/SWNT TFT (Figure S5); and the curve of mobility versus SWNT concentration and the matched function (Figure S6). This material is available free of charge via the Internet at http://pubs.acs.org.

■ AUTHOR INFORMATION

Corresponding Author

*E-mail: liaolei@whu.edu.cn (L.L.) and eezfan@ust.hk (Z.F.).

Notes

The authors declare no competing financial interest.

■ ACKNOWLEDGMENTS

We acknowledges the MOE NCET-10-0643 and NSFC grant (No. 11104207, 91123009, and 10975109), Hubei Province Natural Science Foundation (2011CDB271), the Natural Science of Jiangsu Grant (No. BK2011348), as well as "The Grant of State Key Laboratory of Advanced Technology for Materials Synthesis and Processing (Wuhan University of Technology), General Research Fund (No. 612111) from Hong Kong Research Grant Council. The authors acknowledge helpful discussions with Lianmao Peng, Zhiyong Zhang at Peking University, and Bozhi Tian at the University of Chicago.

■ REFERENCES

(1) Wang, C.; Zhang, J.; Ryu, K.; Badmaev, A.; De Arco, L. G.; Zhou, C. *Nano Lett.* **2009**, *9*, 4285−4291.

(2) Yoo, J. S.; Jung, S. H.; Kim, Y. C.; Byun, S. C.; Kim, J. M.; Choi, N. B.; Yoon, S. Y.; Kim, C. D.; Hwang, Y. K.; Chung, I. J. *J. Dispersion Technol.* **2010**, *6*, 565−570.

(3) Han, L.; Song, K.; Mandlik, P.; Wagner, S. *Appl. Phys. Lett.* **2010**, *96*, 042111.

(4) Nathan, A.; Kumar, A.; Sakariya, K.; Servati, P.; Sambandan, S.; Striakhilev, D. *IEEE J. Solid-State Circuits* **2004**, *39*, 1477−1486.

(5) Bettinger, C. J.; Becerril, H. A.; Kim, D. H.; Lee, B. L.; Lee, S.; Bao, Z. *Adv. Mater.* **2011**, *23*, 1172−1172.

(6) Wang, L.; Yoon, M. H.; Lu, G.; Yang, Y.; Facchetti, A.; Marks, T. J. *Nat. Mater.* **2006**, *5*, 893−900.

(7) Azarova, N. A.; Owen, J. W.; McLellan, C. A.; Grimminger, M. A.; Chapman, E. K.; Anthony, J. E.; Jurchescu, O. D. *Org. Electron.* **2010**, *11*, 1960−1965.

(8) Kim, H. S.; Byrne, P. D.; Facchetti, A.; Marks, T. J. *J. Am. Chem. Soc.* **2008**, *130*, 2580−12581.

(9) Fortunato, E.; Barquinha, P.; Pimentel, A.; Gonçalves, A. M. F.; Marques, A. J. S.; Pereira, L.; Martins, R. F. P. *Adv. Mater.* **2005**, *17*, 590−594.

(10) Song, J. I.; Park, J. S.; Kim, H.; Heo, Y. W.; Lee, J. H.; Kim, J. J.; Kim, G.; Choi, B. D. *Appl. Phys. Lett.* **2007**, *90*, 022106.

(11) Chang, S.; Dong, K. Y.; Park, J. H.; Oh, T. Y.; Kim, J. W.; Lee, S. Y.; Ju, B. K. *Appl. Phys. Lett.* **2010**, *96*, 243504.

(12) Dehuff, N.; Kettenring, E.; Hong, D.; Chiang, H.; Wager, J.; Hoffman, R.; Park, C. H.; Keszler, D. *J. Appl. Phys.* **2005**, *97*, 064505.

(13) Sirringhaus, H.; Bird, M.; Zhao, N. *Adv. Mater.* **2010**, *22*, 3893−3898.

(14) Cherenack, K. H.; Munzenrieder, N. S.; Troster, G. *IEEE Electron Device Lett.* **2010**, *31*, 1254−1256.

(15) Koo, C. Y.; Song, K.; Jun, T.; Kim, D.; Jeong, Y.; Kim, S. H.; Ha, J.; Moon, J. *J. Electrochem. Soc.* **2010**, *157*, J111.

(16) Lee, S. Y.; Chong, E.; Jeon, Y. W.; Kim, D. H. *Appl. Phys. Lett.* **2011**, *98*, 122105.

(17) Sekitani, T.; Zschieschang, U.; Klauk, H.; Someya, T. *Nat. Mater.* **2010**, *9*, 1015−1022.

(18) Yu, M. F.; Files, B. S.; Arepalli, S.; Ruoff, R. S. *Phys. Rev. Lett.* **2000**, *84*, 5552−5555.

(19) Chiang, W. H.; Sankaran, R. M. *Nat. Mater.* **2009**, *8*, 882−886.

(20) Cao, Q.; Rogers, J. A. *Nano Res.* **2008**, *1*, 259−272.

(21) Javey, A.; Guo, J.; Farmer, D. B.; Wang, Q.; Yenilmez, E.; Gordon, R. G.; Lundstrom, M.; Dai, H. *Nano Lett.* **2004**, *4*, 1319–1322.
(22) Servati, P.; Prakash, S.; Nathan, A.; Py, C. *J. Vac. Sci. Technol., A* **2002**, *20*, 1374.
(23) Javey, A.; Guo, J.; Wang, Q.; Lundstrom, M.; Dai, H. *Nature* **2003**, *424*, 654–657.
(24) Kumar, S.; Blanchet, G.; Hybertsen, M.; Murthy, J. Y.; Alam, M. A. *Appl. Phys. Lett.* **2006**, *89*, 143501.
(25) Münzenrieder, N.; Cherenack, K. H.; Tröster, G. *IEEE Trans. Electron Devices* **2011**, 1–8.
(26) Lan, Y.; Peng, W.; Lo, Y.; He, J. *Org. Electron.* **2010**, *11*, 670–676.